Congress on Numerical Methods in Engineering 2011
Coimbra, 14 to 17 June, 2011

CHARACTERIZATION OF THE DYNAMIC INTERACTIONS BETWEEN CARDIOVASCULAR SIGNALS BY CROSS TIME–FREQUENCY ANALYSIS: PHASE DIFFERENCES, TIME DELAY AND PHASE LOCKING

M. Orini[1,2,3*], P. Laguna[1,2], L.T. Mainardi[3] and R. Bailón [1,2]

1: Communications Technology Group (GTC), Aragon Institute of Engineering Research (I3A)
Instituto de Investigación Sanitaria de Aragón
e-mail: michele@unizar.es

2: Centro de Investigación Biomdica en Red en Bioingeniera
Biomateriales y Nanomedicina (CIBER-BBN), Zaragoza

3: Bioengineering department, Politecnico di Milano, Milan, Italy

Keywords: Cardiovascular interactions, Cross time–frequency analysis, Time–frequency coherence, Phase locking, R–R variability, Respiratory signal

Abstract *The study of the dynamic interactions between signals related to the autonomous nervous system can improve the understanding of the underlying mechanisms of the cardiovascular control. In this study, cross time–frequency (TF) analysis is used to estimate the phase differences, the time–delay and the phase locking between cardiovascular signals. Phase differences and time delay give a measure of the changes in the synchronization between two oscillations, while phase locking measures the degree of similarity of these changes across subjects. The presented methodology is based on the smoothed pseudo Wigner–Ville distribution and includes time–frequency coherence analysis.*
In a first simulation study involving highly non–stationary synthetic signals, this methodology provided accurate estimates of the temporal changes of the phase differences, with an error characterized by interquartile ranges lower than 2% and 9% for SNR equal to 20 dB and 0 dB, respectevely. A comparative study showed that the proposed estimator outperformed an estimator based on the integration of the difference between the instantaneous frequency of each spectral component. In a second simulation study, it is shown that the presented methodology reliably followed abrupt time delay changes, with a time of adaptation lower than 10 s.
This methodology was used to characterize the interactions between the RRV and the respiratory signals during tilt table test. In 16 young healthy subjects, head-up tilt caused the phase differences (resp. time delay) to decrease about 0.57 rad (resp. 0.312 s) in HF spectral range, with HF$\in$[0.15, 0.4 Hz]. During the test, the phase locking estimated in HF range, fluctuated around 0.64$\pm$0.11 and slightly decreased during head-up tilt, from 0.67$\pm$0.11 to 0.61$\pm$0.11, thus indicating a higher variability across subjects in the coupling during head-up tilt.

1 INTRODUCTION

To introduce the time–frequency phase differences (TFPD) and the time–frequency phase locking (TFPL), let's write a simple model for the analytic representation of cardiovascular signals, as the sum of complex exponentials showing both amplitude and frequency modulation, embedded in noise:

$$\begin{cases} x(t) = & A_{\mathrm{x,LF}}(t)e^{i\theta_{\mathrm{x,LF}}(t)} + A_{\mathrm{x,HF}}(t)e^{i\theta_{\mathrm{x,HF}}(t)} + w_{\mathrm{x}}(t) \\ y(t) = & A_{\mathrm{y,LF}}(t)e^{i\theta_{\mathrm{y,LF}}(t)} + A_{\mathrm{y,HF}}(t)e^{i\theta_{\mathrm{y,HF}}(t)} + w_{\mathrm{y}}(t) \end{cases} \tag{1}$$

In this expression LF and HF indicate the low frequency component, LF∈[0.04, 0.15 Hz], and the high frequency component, HF∈[0.15, 0.4 Hz], respectively; $\theta_{\mathrm{k,B}}(t)$, with B∈[LF,HF] and $k \in [x,y]$, is the instantaneous phase, related to the instantaneous frequency by $f_{\mathrm{k,B}}(t) = (d\theta_{\mathrm{k,B}}(t)/dt)/(2\pi)$; $w_{\mathrm{k}}(t)$ is a white Gaussian noise (WGN). As cardiovascular signals are usually non–stationary, the phase difference between each spectral component, $\theta_{\mathrm{B}}(t) = \theta_{\mathrm{x,B}}(t) - \theta_{\mathrm{y,B}}(t)$, is expected to be time–varying. An illustrative example of two synthetic signals which share similar instantaneous frequencies and are characterized by time–varying phase differences, is shown in Fig. 1. This example may represent LF oscillations of R–R variability (RRV) and systolic arterial pressure variability (SAPV) during non–stationary conditions. The estimation of the TFPD spectrum, which quantifies the changes in the synchronization between two oscillations, and the TFPL, which measures the degree of similarity of these changes across subjects, can reveal valuable information to characterize the dynamic interactions between signals related to the cardiovascular and cardiorespiratory systems.

The estimation of phase differences between biomedical non–stationary signals in the joint TF domain was used in few studies [1, 2, 3, 4, 5]. Among them, no one focuses on the characterization of cardiovascular dynamics. From a methodological viewpoint, TFPD has been estimated by wavelet transform [2, 3], by Rihaczek transform [1] and by reduced interference distributions [6].

The purpose of this study is to describe a robust technique to accurately estimate the TFPD and TFPL via smoothed pseudo Wigner–Ville distribution (SPWVD), and to show the usefulness of such approach in the analysis of the cardiovascular and cardiorespiratory system. The presented methodology is assessed in simulation studies and is used to characterize the dynamic interactions between the RRV and respiratory signals during tilt table test.

2 METHODS

Given (1), the time–course of the phase difference between two signals, evaluated for a specific spectral component *B*, can be estimated as:

$$\hat{\theta}_{\mathrm{B}}(t) = 2\pi \int_0^{\mathrm{t}} [f_{\mathrm{x,B}}(\tau) - f_{\mathrm{y,B}}(\tau)]d\tau \tag{2}$$

This procedure has two main drawbacks: it is very sensitive to estimation errors in $f_{\mathrm{k,B}}(t)$, since an estimation error at t_0 affects all $\hat{\theta}_{\mathrm{B}}(t > t_0)$, and gives a quantification of the phase differences

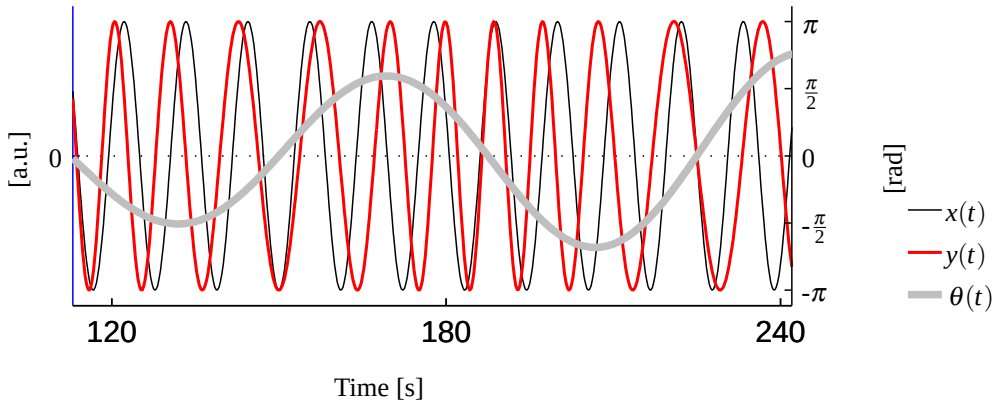

Figure 1: Example of signals oscillating at typical Mayer wave frequency and characterized by time–varying phase differences $\theta(t)$

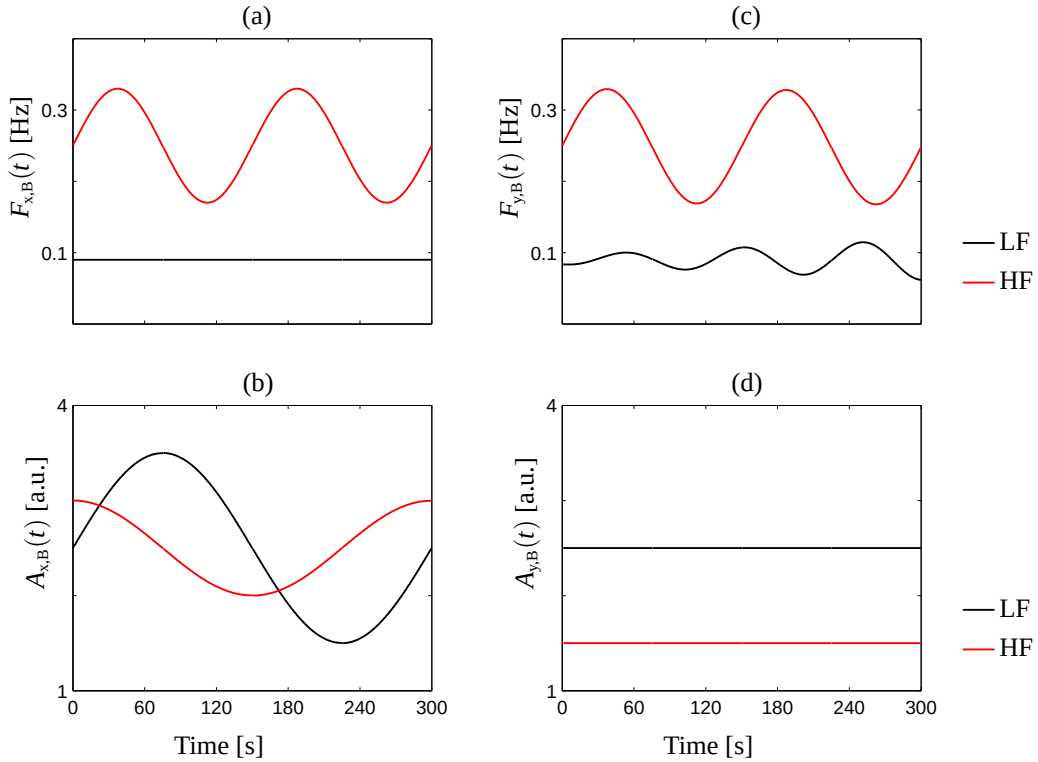

Figure 2: Time–frequency structure of signals of type (1) used in the simulation studies. (a)–(b): Instantaneous frequencies, (c)–(d): instantaneous amplitudes of signals $x(t)$ and $y(t)$, respectively. Time–course of LF and HF spectral indices are in black and red, respectevely.

only at $f_{k,B}(t)$. In cardiovascular signal analysis, these inconveniences are particularly serious, since biomedical signals are never perfectly narrow–band and an accurate estimation of the instantaneous frequencies is not always possible.
Cross TF analysis provides a simultaneous characterization of the phase differences in time and frequency, and allows to overcome these limitations. The presented methodology is based on the estimation of the TFPD spectrum, from which the time–course of the phase difference between each spectral component is extracted. It is composed of the following steps:

(i) Estimation of auto and cross TF spectra, $\hat{S}_{xx}(t,f)$, $\hat{S}_{yy}(t,f)$ and $\hat{S}_{xy}(t,f)$,via SPWVD [7, 8]:

$$\hat{S}_{xy}(t,f) = \iint_{-\infty}^{\infty} \Phi(\tau,\nu) A_{xy}(\tau,\nu) e^{j2\pi(t\nu-\tau f)} d\nu d\tau \tag{3}$$

$$A_{xy}(\tau,\nu) = \int_{-\infty}^{\infty} x\left(t+\frac{\tau}{2}\right) y^*\left(t-\frac{\tau}{2}\right) e^{-j2\pi\nu t} dt \tag{4}$$

$$\Phi(\tau,\nu;\tau_0,\nu_0,\lambda) = \exp\left\{-\pi\left[\left(\frac{\nu}{\nu_0}\right)^2 + \left(\frac{\tau}{\tau_0}\right)^2\right]^{2\lambda}\right\} \tag{5}$$

where $A_{xy}(\tau,\nu)$ is the cross ambiguity function and $\Phi(\tau,\nu)$ is a smoothing kernel function [9], already used in cross TF analysis of cardiovascular signals [8, 10, 11].

(ii) Estimation of the TFPD spectrum, $\hat{\Theta}(t,f)$, and TF coherence, $\hat{\gamma}(t,f)$:

$$\hat{\Theta}(t,f) = \arctan\left[\frac{\Im\left[\hat{S}_{xy}(t,f)\right]}{\Re\left[\hat{S}_{xy}(t,f)\right]}\right];\ \hat{\Theta}(t,f) \in [-\pi,\pi] \tag{6}$$

$$\hat{\gamma}(t,f) = \frac{\left|\hat{S}_{xy}(t,f)\right|}{\sqrt{\hat{S}_{xx}(t,f)\hat{S}_{yy}(t,f)}};\ \ \hat{\gamma}(t,f) \in [0,1] \tag{7}$$

(iii) Localization of the TF regions where the coherence is statistically significant. This is done by a hypothesis test, based on the comparison of $\hat{\gamma}(t,f)$ with a threshold function $\gamma_{TH}(t,f)$, obtained as the 95th percentile of the statistical distribution $\Gamma(t,f) = \{\hat{\gamma}_1(t,f),...,\hat{\gamma}_j(t,f),...\}$, where $\hat{\gamma}_j(t,f)$ is the TFC between the jth realization of two WGNs. The estimation of the threshold as the 95th percentile of $\Gamma(t,f)$ is associated to a significance level (type I error) of 5%. The regions where the TF coherence is significant, $\Omega_B^{(\gamma)}$, are defined as:

$$\Omega_B^{(\gamma)} = \left\{(t,f) \in (\mathbb{R}^+ \times B) \mid \hat{\gamma}(t,f) > \gamma_{TH}(t,f)\right\};\ \text{with } B = \{LF, HF\} \tag{8}$$

(iv) Identification of the TF regions, $\Omega_B^{(\theta)}$, in which the time–course of the phase difference between each spectral component is estimated. To localize these TF regions, the instantaneous frequency which corresponds to the maximum of the magnitude of the cross TF

spectrum, evaluated inside $\Omega_{\mathrm{B}}^{(\gamma)}$ is estimated as:

$$f_{\mathrm{B}}^{(\theta)}(t) = \arg\left[\max_{f\in\Omega_{\mathrm{B}}^{(\gamma)}}\left[\left|\hat{S}_{\mathrm{xy}}(t,f)\right|\right]\right] \tag{9}$$

Regions $\Omega_{\mathrm{B}}^{(\theta)}$, with $\Omega_{\mathrm{B}}^{(\theta)} \subseteq \Omega_{\mathrm{B}}^{(\gamma)}$, are centered around $f_{\mathrm{B}}^{(\theta)}(t)$ and are defined as:

$$\Omega_{\mathrm{B}}^{(\theta)} = \left\{(t,f) \in \Omega_{\mathrm{B}}^{(\gamma)} \mid f = f_{\mathrm{B}}^{(\theta)}(t) \pm \frac{\Delta_{\mathrm{f}}}{2}\right\} \tag{10}$$

where Δ_{f} is a term related with the frequency resolution of the TF distributions, which determines the maximum width of $\Omega_{\mathrm{B}}^{(\theta)}$. Parameter Δ_{f} is estimated as the full width at half maximum of the function $\phi(t=0,f)$, where $\phi(t,f)$ is the two dimensional Fourier transform of (5):

$$\phi(t,f) = \iint \Phi(\tau,\nu) e^{i2\pi(t\nu-\tau f)} d\tau d\nu \tag{11}$$

(v) The time–course of the phase differences between each spectral component of the two signals, $\hat{\theta}_{\mathrm{B}}(t)$, is finally estimated (in radians) by averaging the TFPD spectrum in $\Omega_{\mathrm{B}}^{(\theta)}$:

$$\hat{\theta}_{\mathrm{B}}(t) = \left[\int_{\Omega_{\mathrm{B}}^{(\theta)}} \Theta(t,f) df\right] \Big/ \left[\int_{\Omega_{\mathrm{B}}^{(\theta)}} 1 df\right];\ \ B \in \{LF, HF\} \tag{12}$$

The time delay associated to $\hat{\theta}_{\mathrm{B}}(t)$ can be estimated (in seconds) as:

$$\hat{\mathscr{D}}_{\mathrm{B}}(t) = \frac{\hat{\theta}_{\mathrm{B}}(t)}{2\pi f_{\mathrm{B}}^{(\theta)}(t)} \tag{13}$$

The degree of phase–locking between different couples of signals [1] is estimated, on the whole population, by the TFPL:

$$\hat{\Psi}(t,f) = \left|\frac{1}{L}\sum_{j=1}^{L} e^{i2\pi\hat{\Theta}_{\mathrm{j}}(t,f)}\right|,\ \ \hat{\Psi}(t,f) \in [0,1] \tag{14}$$

where L is the number of subjects. For a given TF point, $\hat{\Psi}(t,f)$=1 if at that point the phase differences are the same for all subjects, while $\hat{\Psi}(t,f)$=0 if the phase differences randomly change across subjects.

3 VALIDATIONS

Two simulation studies were carried on with the purpose of validating the proposed methodology and comparing its performance with a traditional estimator not based on cross TF analysis. In particular, these simulations aim at assessing, in illustrative examples, the tracking capability and the robustness against noise of the estimators. Simulated signals are of type (1)

and are characterized by the highly non–stationary TF structure reported in Fig. 2. These signals can be seen as locally coupled, since their spectral components share similar instantaneous frequencies and their amplitudes vary slowly. From a physiological viewpoint, the time–course of the instantaneous frequencies of the HF components, $f_{x,HF}(t)$ and $f_{y,HF}(t)$, covers the range of possible respiratory frequencies observed in many autonomic tests, and it may correspond to the pattern of the respiratory frequency observed during some respiratory disorders such as periodic breathing. From a theoretic viewpoint, the tracking of time–varying spectral components characterized by sinusoidal frequency modulation is challenging, due to the high level of inner interference terms which characterizes signals with such a modulation [12].

Simulation I – phase differences: The performance of the estimator of phase differences based on cross TF analysis, described through (3)–(12), is compared to the performance of the estimator based on the integration of the instantaneous frequencies, described in (2). The time–course of the phase difference between each spectral component of $x(t)$ and $y(t)$, i.e. $\theta_B(t) = \theta_{y,B}(t) - \theta_{x,B}(t)$, are reported in Fig. 3a–b. These phase differences cause the instantaneous frequencies of the signals to slightly differ. In this simulation, the tracking of the phase differences is particularly challenging since all the parameters which determine the TF structure of the signals, i.e. $A_{k,B}$(t), $f_{k,B}(t)$ and $\theta_B(t)$, vary quickly and simultaneously. In particular, the most abrupt changes occur in LF, where the rate of variation of $\theta_{LF}(t)$ gives, for $t \approx$260 s, $|f_{x,LF}(t) - f_{y,LF}(t)| \approx 0.028$ Hz.

Simulation II – time delay: In this simulation, the performance of the proposed methodology in tracking the time delay, given in (13), is assessed. Signal $y(t)$ is obtained from signal $x(t)$, whose TF structure is the same as that used in the previous simulation (see Fig. 2a–b), as $y(t) = x(t + \mathscr{D}(t))$. Time delay $\mathscr{D}(t)$ increased stepwise as shown in Fig. 4.

4 PHYSIOLOGICAL STUDY

Signals were recorded from 16 young healthy subjects (age 29±3 years) during a tilt table test with a protocol already illustrated in [10]. The experimental protocol consisted of: 4 minutes in early supine position (W_1), 5 minutes tilted head–up to an angle of 70^o (W_2) and 4 minutes back to later supine position (W_3). During head–up tilt, subjects undergo a progressive orthostatic stress. The ECG and respiratory signals were recorded using the Biopac MP 150 system with a sampling frequency of 1 kHz and 125 Hz, respectively. The QRS complexes in the ECG were detected and the RR signal was obtained by using a method based on the integral pulse frequency modulation model, which accounts for the presence of ectopic beats and artifacts [13]. The RR and the respiratory signals were resampled at 4 Hz and the RRV signals was obtained by high–pass filtering the corresponding series with a cut–off frequency of 0.03 Hz.

5 RESULTS

5.1 Simulation studies

Time–frequency spectra were estimated by using the kernel (5), which gave a time and frequency resolution of about 12 s and 0.04 Hz. In both simulations, the estimation of $\theta_B(t)$ and $\mathscr{D}(t)$ was repeated for different level of SNR, going from 20 to 0 dB. For every SNR level, 100 couples of signals were processed. The results of the first simulation are summarized in Fig. 3, where panels (a)–(d) and (e)–(h) show the results obtained by cross TF analysis as in (12), and by integration of the differences of the instantaneous frequencies, as in (2), respectively. In (2), the instantaneous frequencies of the spectral components of $x(t)$ and $y(t)$ were estimated as the frequencies corresponding to the maximum of the instantaneous auto TF spectra in both LF and HF bands. The time–course of the estimated phase differences between each component, $\hat{\theta}_B(t)$, is shown in panels (a)–(b) and (e)–(f), where results are given as the range between the lower and upper quartiles of the estimates. As shown, the estimator based on cross TF analysis gave a better characterization of the changes of the phase differences than the estimator based on the estimation of the instantaneous frequencies. To quantify the goodness of the estimation, the median, and the lower and upper quartiles of the estimation errors, $\theta_B(t) - \hat{\theta}_B(t)$, were calculated for every iteration. The results of error analysis are given in Fig. 3c–d and Fig. 3g–h, where circles and bars represent the average of the median and of the interquartile ranges of the estimation errors. Numerical results are given in Table 1. Concerning the results obtained by cross TF analysis, it is shown that the median errors were always lower than 0.013 rad, even for SNR as low as 0 dB. The variability of the estimation depended on the SNR and on the rate of variation of $\theta_B(t)$. For SNR=20 dB and for $\theta(t)$ varying quadratically, as in $\theta_{HF}(t)$, the interquartile ranges were lower than 0.05 rad, less than 2% of the total range of variation of $\theta(t)$. For SNR=0 dB and for $\theta(t)$ varying sinusoidally, as in $\theta_{LF}(t)$, the interquartile range was about 0.42 rad, about 8% of the total range of variation of $\theta(t)$.

The estimation of the phase differences by integration of the differences between the instantaneous frequencies gave results characterized by much lower accuracy. The estimation errors were characterized by interquartile ranges at least 34% higher than those obtained by cross TF analysis. For SNR equal to 0 dB, the interquartile ranges of the errors given by (2) were, in LF and HF bands, more than 200% and 800% higher than those obtained by the proposed method. The lower accuracy in estimating the phase differences by (2) with respect to (12), was mainly due to the difficulty of perfectly tracking the instantaneous frequencies of the signals, specially in presence of noise.

Results of the simulation II are reported in Fig. 4 and Table 1. In this simulation, the time delay $\hat{\mathscr{D}}_B(t)$ is estimated only by cross TF analysis, as in (13). In Fig. 4a–b, it is shown that the median trend of the estimates correctly tracked the abrupt changes of $\mathscr{D}_B$, with a time of adaptation, from the stepwise increase of $\mathscr{D}_B(t)$ to the stabilization of the estimates, of about 10 s. As shown in Table 1, the variability of the estimates is greatly affected by the level of the noise and is higher in LF.

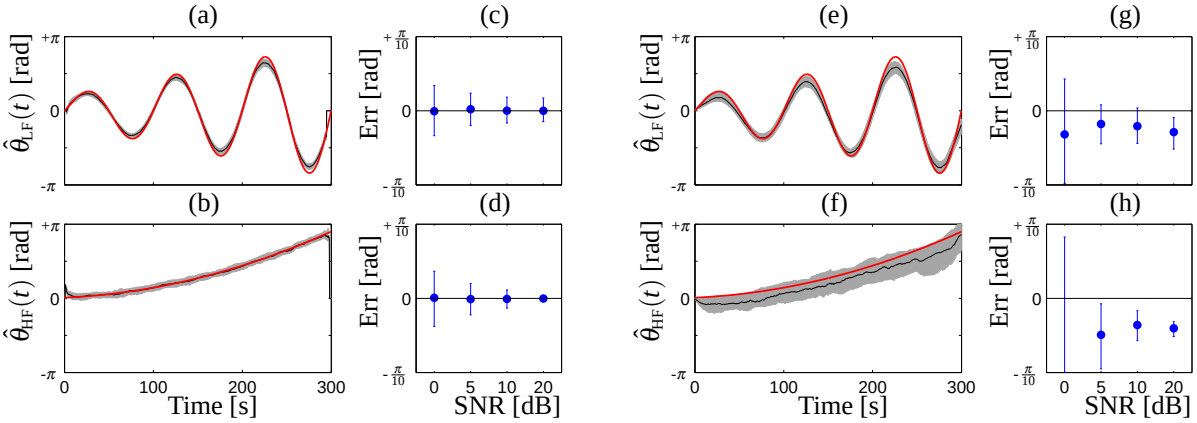

Figure 3: Simulation I. (a)–(d): results of the proposed methodology based on cross TF analysis; (e)–(h): results obtained by instantaneous frequency estimates. (a)–(b) and (e)–(f): red lines represent $\theta(t)$; shadowed areas represent the range between the lower and upper quartile of estimates $\hat{\theta}(t)$. In these examples SNR=10 dB; (c)–(d) and (g)–(h): circles and bars represent the average of the I, II and III quartiles of the estimation errors.

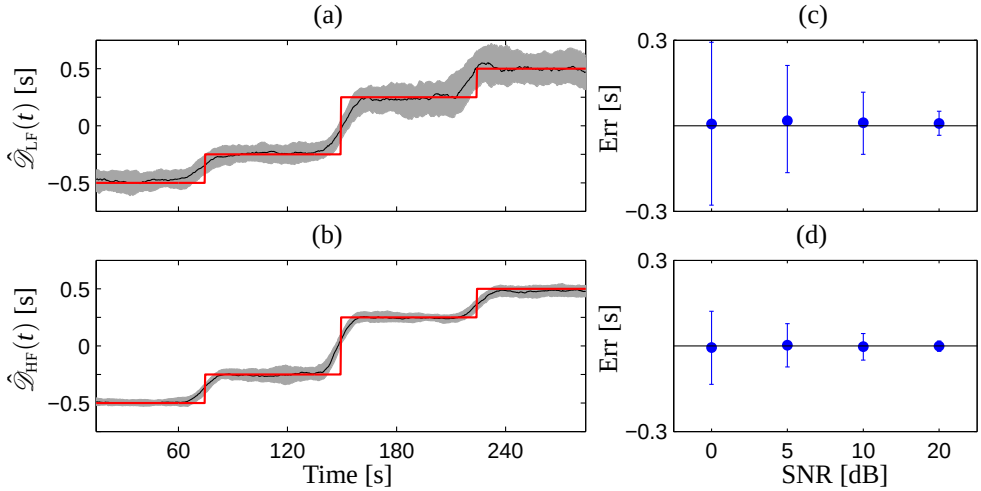

Figure 4: Simulation II – Time delay estimation (a)–(b): results of the proposed methodology based on cross TF analysis; red lines represent $\mathscr{D}_{\text{B}}(t)$; shadowed areas represent the range between the lower and upper quartile of estimates $\hat{\mathscr{D}}_{\text{B}}(t)$. In these examples SNR=10 dB; (c)–(d): circles and bars represent the average of the I, II and III quartiles of the estimation errors.

Param	(eq.)	[unit]	20 dB	10 dB	5 dB	0 dB
$\hat{\theta}_{\mathrm{LF}}(t)$	(12)	[Hz]	0.000 $\pm$ 0.200	0.000 $\pm$ 0.220	0.013 $\pm$ 0.274	-0.004 $\pm$ 0.426
	(2)	[Hz]	-0.180 $\pm$ 0.268	-0.131 $\pm$ 0.300	-0.113 $\pm$ 0.331	-0.201 $\pm$ 0.886
$\hat{\theta}_{\mathrm{HF}}(t)$	(12)	[Hz]	-0.001 $\pm$ 0.049	-0.006 $\pm$ 0.153	-0.007 $\pm$ 0.264	0.005 $\pm$ 0.468
	(2)	[Hz]	-0.254 $\pm$ 0.126	-0.23 $\pm$ 0.253	-0.309 $\pm$ 0.551	-1.719 $\pm$ 3.923
$\hat{\mathscr{D}}_{\mathrm{LF}}(t)$	(13)	[sec]	0.008 $\pm$ 0.084	0.011 $\pm$ 0.218	0.017 $\pm$ 0.376	0.006 $\pm$ 0.571
$\hat{\mathscr{D}}_{\mathrm{HF}}(t)$	(13)	[sec]	0.000 $\pm$ 0.036	-0.002 $\pm$ 0.093	0.003 $\pm$ 0.151	-0.006 $\pm$ 0.256

Table 1: Simulation results. Results are reported as the average of the median $\pm$ the interquartile range of the estimation errors obtained at each iteration. From top to bottom, results concern the estimation errors shown in Fig. 3c, 3d, 3g, 3h, 4c, 4d.

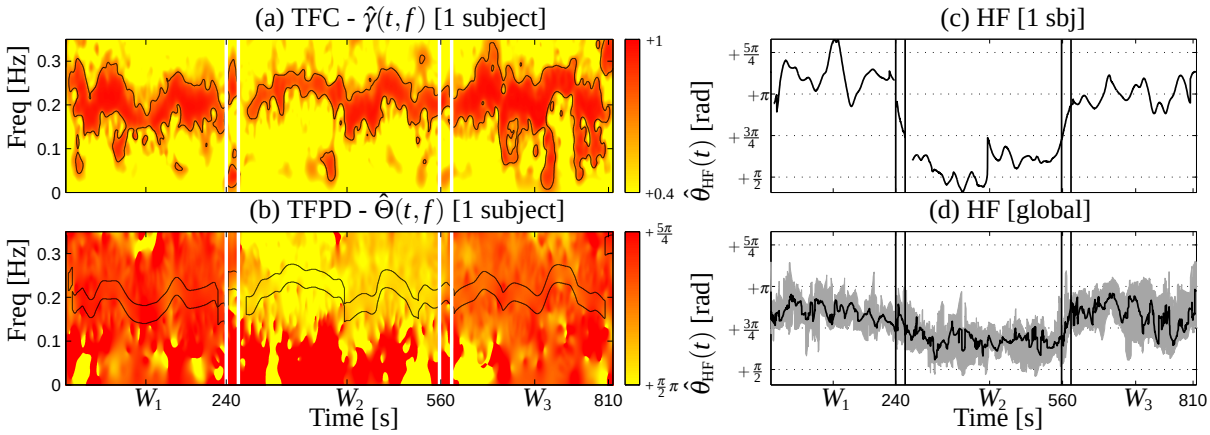

Figure 5: Phase differences between RRV and respiratory signal during tilt table test. Vertical lines mark the early supine position, the head–up tilt and the later supine position. (a)–(c): Results from a subject. (d): Global results. (a): black contours encircled the regions where the TFC was statistically significant. (b): black contours represent $\Omega_{\mathrm{B}}^{(\theta)}$. (c) phase difference between the HF component, estimated by averaging $\Theta(t,f)$ in $\Omega_{\mathrm{HF}}^{(\theta)}$. (d) Global trends: lines represent the median values and the shadowed area the interval between the lower and upper quartile.

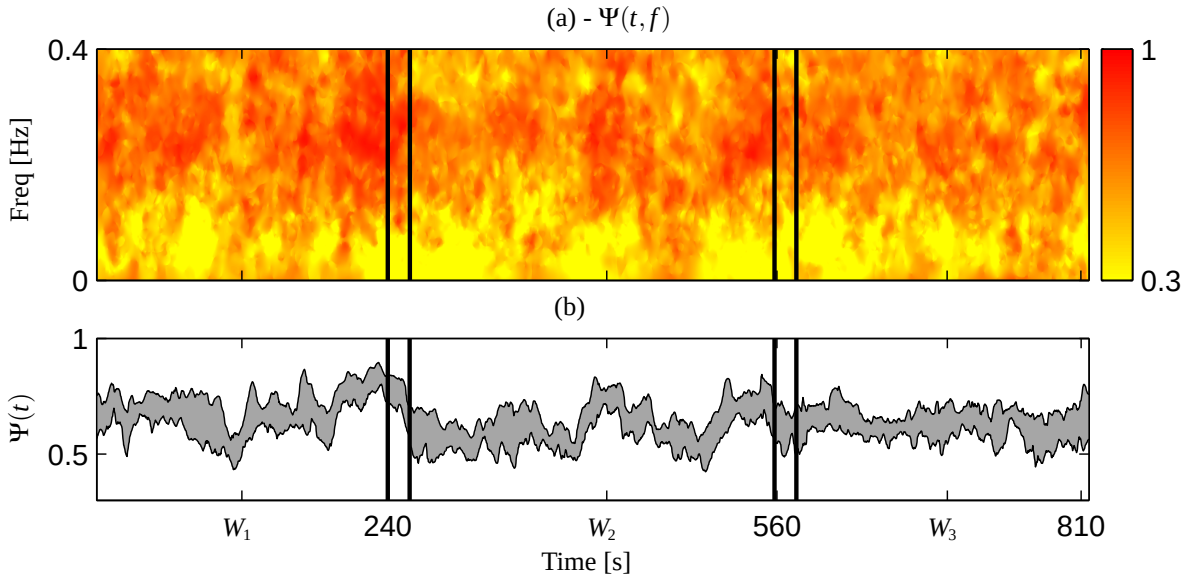

Figure 6: (a): Time–frequency phase locking, $\Psi(t,f)$, between the RRV and the respiratory signal estimated in 14 subjects undergoing tilt table test. (b): Interval between the I and III quartiles of $\Psi(t,f)$, estimated along f.

5.2 Physiological study

An illustrative example of the estimation of the phase differences between the RRV and the respiratory signals is shown in Fig. 5. In Fig. 5a it is shown that, despite the non–stationary structure of the signals, by TF coherence analysis was possible to localize regions in which coherence was statistically significant. These regions, $\Omega_{\text{B}}^{(\gamma)}$, are encircled by a black contour. In Fig. 5b it is shown that the TFPD spectrum was everywhere close to π. Given that the spectral content of the respiratory signal usually lies in HF, only results concerning $\hat{\theta}_{\text{HF}}(t)$ are shown. Parameter $\hat{\theta}_{\text{HF}}(t)$ was estimated by averaging the TFPD in $\Omega_{\text{HF}}^{(\theta)}$, whose boundaries are reported in Fig. 5b. In Fig. 5c, it is shown that for this subject, the movement back and forth from supine position to head–up tilt provoked almost instantaneous changes in $\hat{\theta}_{\text{HF}}(t)$, which during tilt decreased more than $\pi/2$ and then, when supine position was restored, went back to values similar to those observed in early supine position. These changes in the phase differences corresponded to a change in the time delay $\mathscr{D}_{\text{HF}}(t)$, whose mean trend decreased 1.57 s, from 2.89 s in early supine position to 1.32 s during tilt. Note that this subject showed particularly high changes of both phase differences and time delay.

Results concerning the global trends of the study population are shown in Fig. 5d, where lines represent the instantaneous median values of $\hat{\theta}_{\text{HF}}(t)$ and shadowed areas the lower and upper quartiles, estimated among subjects. In the whole study population, the head–up tilt caused the phase differences to decrease about 0.55 rad in HF, being the median trend equal to 2.70$\pm$0.14 rad in W_1, 2.12$\pm$0.13 rad in W_2, 2.61$\pm$0.24 rad in W_3. On average, during the head–up tilt, the time delay $\mathscr{D}_{\text{B}}(t)$ decreased 0.272 s, being the median trend equal to 1.60$\pm$0,20 s (W_1), 1.33$\pm$

0.19 s (W_2) and 1.46±0.28 s (W_3).
The TFPL, shown in Fig. 6a, fluctuated around 0.64±0.11 in HF and 0.44±0.15 in LF. The median trend and the interquartile range of the TFPL, evaluated in HF, are shown in Fig. 6b. In HF, the median trend of the TFPL was equal to 0.67±0.07 (W_1), 0.61±0.07 (W_2) and 0.63±0.03 (W_3). Although the phase differences $\hat{\theta}_{\mathrm{HF}}(t)$ followed a common pattern, shown in Fig. 5d, the phase locking, evaluated in HF, is not high and slightly decreased during head–up tilt, thus indicating a higher variability across subjects in the coupling during W_2. The low values of the TFPL are likely due to the fact that the common pattern of $\hat{\theta}_{\mathrm{HF}}(t)$ took place, for every subject, in different portions of the TF domain. This shown the importance of the localization of specific TF regions, $\Omega_{\mathrm{B}}^{(\gamma)}$, to properly estimate the time–course of the phase differences.

6 DISCUSSION

In this study, a new methodology for the quantification of phase differences in non–stationary signals related to the cardiovascular and cardiorespiratory systems, based on cross TF analysis, is proposed. This methodology includes the estimation of the temporal changes of the phase differences, the time delay and the phase locking. The SPWVD provides auto and cross spectra characterized by high joint TF resolution [8], which can be independently adjusted in time and frequency. Moreover, the localization of TF regions where spectral coherence is statistically significant (i.e., where signals are sharing similar instantaneous frequencies) allows to robustly estimate the phase differences and the time delay. The localization of these TF regions is of crucial importance to reliably extract the time–course of the phase differences from the TFPD spectrum.
In non–stationary context, this methodology was shown to provide accurate estimates also in presence of noise, and it outperformed techniques based on instantaneous frequency estimates. Finally, the TF representation of the phase-locking between different couples of signals allows to assess whether a determined stimulus provokes, among different subjects, similar patterns of synchronization. The analysis of signals recorded during tilt table test shows that head–up tilt provoked changes in the phase differences between RRV and the respiratory signals. The presented methodology provides a characterization of cardiovascular interactions which may add valuable information toward a better understanding of the dynamics involved in the cardiovascular control.

7 Acknowledgment

This study was supported by Ministerio de Ciencia e Innovación, Spain, under Project TEC2010-21703-C03-02 and TRA2009-0127, in part by the Diputación General de Aragón (DGA), Spain, through Grupos Consolidados GTC ref:T30, by ISCIII, Spain, through CIBER CB06/01/0062.

REFERENCES

[1] S. Aviyente, E. M. Bernat, W. S. Evans, and S. R. Sponheim, "A phase synchrony measure for quantifying dynamic functional integration in the brain." *Hum Brain Mapp*, pp. 80–93, Mar 2010.

[2] L. Cnockaert, P.-F. Migeotte, L. Daubigny, G. K. Prisk, F. Grenez, and R. C. S, "A method for the analysis of respiratory sinus arrhythmia using continuous wavelet transforms." *IEEE Trans Biomed Eng*, vol. 55, no. 5, pp. 1640–1642, May 2008.

[3] J.-P. Lachaux, A. Lutz, D. Rudrauf, D. Cosmelli, M. L. V. Quyen, J. Martinerie, and F. Varela, "Estimating the time-course of coherence between single-trial brain signals: an introduction to wavelet coherence." *Neurophysiol Clin*, vol. 32, no. 3, pp. 157–174, Jun 2002.

[4] D. Li and R. Jung, "Quantifying coevolution of nonstationary biomedical signals using time-varying phase spectra." *Ann Biomed Eng*, vol. 28, no. 9, pp. 1101–1115, Sep 2000.

[5] J. P. Lachaux, E. Rodriguez, J. Martinerie, and F. J. Varela, "Measuring phase synchrony in brain signals." *Hum Brain Mapp*, vol. 8, no. 4, pp. 194–208, 1999.

[6] Y.-J. Shin, D. Gobert, S.-H. Sung, E. J. Powers, and J. B. Park, "Application of cross time-frequency analysis to postural sway behavior: the effects of aging and visual systems." *IEEE Trans Biomed Eng*, vol. 52, no. 5, pp. 859–868, May 2005.

[7] F. Hlawatsch and G. F. Boudreaux-Bartels, "Linear and quadratic time-frequency signal representations," *Signal Processing Magazine, IEEE*, vol. 9, no. 2, pp. 21–67, April 1992.

[8] M. Orini, R. Bailón, L. T. Mainardi, A. Minchole, and P. Laguna, "Continuous quantification of spectral coherence using quadratic time-frequency distributions: Error analysis and application," in *Proc. Computers in Cardiology*, 2009, pp. 681–684.

[9] A. Costa and G. Boudreau-Bartels, "Design of time-frequency representations using a multiform, tiltable exponential kernel," *Signal Processing, IEEE Transactions on*, vol. 43, no. 10, pp. 2283–2301, Oct 1995.

[10] E. Gil, M. Orini, R. Bailón, J. M. Vergara, L. Mainardi, and P. Laguna, "Photoplethysmography pulse rate variability as a surrogate measurement of heart rate variability during non-stationary conditions." *Physiol Meas*, vol. 31, no. 9, pp. 1271–1290, Sep 2010.

[11] M. Orini, L. T. Mainardi, E. Gil, P. Laguna, and R. Bailón, "Dynamic assessment of spontaneous baroreflex sensitivity by means of time-frequency analysis using either rr or pulse interval variability." *Conf Proc IEEE Eng Med Biol Soc*, vol. 1, pp. 1630–1633, 2010.

[12] F. Hlawatsch and P. Flandrin, *The Wigner Distribution - theory and applications in signal processing*. Elsevier, 1997, ch. The interference structure of the Wigner distribution and related time-frequency signal representations, pp. 59–113.

[13] J. Mateo and P. Laguna, "Analysis of heart rate variability in the presence of ectopic beats using the heart timing signal," *IEEE Trans Biomed Eng*, vol. 50, no. 3, pp. 334–343, March 2003.